Article

Self-Assembled Triphenylphosphonium-Conjugated Dicyanostilbene Nanoparticles and Their Fluorescence Probes for Reactive Oxygen Species

Wonjin Choi [1,†], Na Young Lim [1,†], Heekyoung Choi [1], Moo Lyong Seo [1,*], Junho Ahn [2,*] and Jong Hwa Jung [1,*]

[1] Department of Chemistry and Research Institute of Natural Science, Gyeongsang National University, Jinju 52828, Korea; cwj1685@gnu.ac.kr (W.C.); skdud325@gnu.ac.kr (N.Y.L.); smile377@gnu.ac.kr (H.C.)
[2] Composites Research Division, Korea Institute of Materials Science, Changwon 51508, Korea
* Correspondence: mlseo@gnu.ac.kr (M.L.S.); junho2587@kims.re.kr (J.A.); jonghwa@gnu.ac.kr (J.H.J.); Tel.: +82-55-772-1488 (J.H.J.)
† These authors contributed equally to this work.

check for updates

Abstract: We report self-assembled novel triphenylphosphonium-conjugated dicyanostilbene- based as selective fluorescence turn-on probes for $^1O_2$ and ClO^-. Mono- or di-triphenylphosphonium-conjugated dicyanostilbene derivatives **1** and **2** formed spherical structures with diameters of ca. 27 and 56.5 nm, respectively, through π-π interaction between dicyanostilbene groups. Self-assembled **1** showed strong fluorescent emission upon the addition of $^1O_2$ and ClO^- compared to other ROS ($O_2{}^-$, •OH, NO, TBHP, H_2O_2, GSH), metal ions (K^+, Na^+), and amino acids (cysteine and histidine). Upon addition of $^1O_2$ and ClO^-, the spherical structure of **1** changed to a fiber structure (8-nm wide; 300-nm long). Upon addition of $^1O_2$ and ClO^-, the chemical structural conversion of **1** was determined by FAB-Mass, NMR, IR and Zeta potential analysis, and the strong emission of the self-assembled **1** was due to an aggregation-induced emission enhancement. This self-assembled material was the first for selective ROS as a fluorescence turn-on probe. Thus, a nanostructure change-derived turn-on sensing strategy for $^1O_2$ or ClO^- may offer a new approach to developing methods for specific guest molecules in biological and environmental subjects.

Keywords: dicyanostilbene; triphenylphosphonium; self-assembly; ROS detection

1. Introduction

Generally, self-assembly of aggregation-induced emission (AIE)-active molecules in aqueous solution depends on intermolecular hydrogen bonding, π-π stacking, and hydrophobic interactions that form nanoscale architectures, such as spheres, rods, and fibers, with fluorescence enhancement [1,2]. Nanostructures formed via molecular self-assembly involving stimuli-responsive properties have great potential for biological and environmental applications [3–6]. Despite the utilization of dual effects on fluorescence turn-on originating from intramolecular electron transfer and intermolecular self-assembly [7], fluorogenic or chromogenic sensing of biologic or environmental species with selective turn-on detection have rarely been reported due to the difficulty associated with the design and synthesis of fluorescence probes. Strong interactions between acidic protons and solvent molecules cause act as a fluorescence quenching factor by photoelectron transfer (PET). Therefore, the self-assembled AIE fluorescence probes with hydrophobic positive charge are useful as sensing materials in biological field [8–10].

Studies related to optical detection using chromogenic or fluorogenic chemoprobes have been performed for biological and environmental applications of singlet oxygen ($^1O_2$) and hypochlorite

(ClO⁻), such as the main component of a cleaning agent for industrial wastewater and cancer treatments that destroy tumor cells [11–13]. Fluorescent probes that demonstrate rapid response, high sensitivity, and technical simplicity are attractive tools for analyte monitoring [14], and fluorescent probes with a reaction-induced signal have been designed to detect a specific signal for singlet oxygen or hypochlorite [15]. In addition, a variety of fluorescent probes for ROS detection have been reported [11,16]. For example, a probe for singlet oxygen primarily produced detection signals by the addition reaction of singlet oxygen to anthracene or the rhodamine backbone [17,18]. In addition, an Ir (III) complex-linked coumarin 314 derivative has been used to identify a ratiometric signal through $^1O_2$-mediated abstraction of the α-H from the tertiary amine [19]. In a probe for hypochlorite detection, fluorescent probe reactions with hypochlorite, such as oxidative cleavage reaction of double bonds (C=C, C=S, C=N, and N=N) or oxidative–hydrolysis reaction of amide, diphenyl ether, and thioether, produced detection signals from the reaction product [20].

In particular, depending on the self-assembly conditions, amphiphilic molecules with AIE have attracted significant attention due to the ease of controlling the fluorescence of an aggregate, which facilitates the construction of fluorescent turn off-on systems [21]. To obtain fluorescence turn-on signals by the reaction of a probe with an analyte, AIE molecules, such as tetraphenylethylene (TPE), are typically applied for ROS detection [22]. Dicyanodistyrylbenzenes are p-conjugated molecules with various optical properties, such as AIE in emission properties and tunable luminescence emission [23]. Compared to homologous a-cyanostilbenes, emission spectra occur at higher wavelengths due to their longer conjugation length [24]. Therefore, dicyanostilbene-linked amphiphilic molecules are a promising turn-on fluorescent sensor for singlet oxygen ($^1O_2$) and hypochlorite (ClO⁻). Thus, we designed triphenylphosphonium (TPP)-conjugated dicyanostilbene derivatives as amphiphilic molecules for turn-on detection of singlet oxygen ($^1O_2$) and hypochlorite (ClO⁻). TPP lipophilic cations were linked to dicyanostilbene to construct more rigid nanostructures in aqueous solution (i.e., the lipophilic cations enhance the stability of organic nanostructures by preventing solvent hydration and providing temperature or pH resistance) [25]. Here, we report the self-assembly properties of mono- or di-TPP-conjugated dicyanostilbene derivatives (**1** and **2**) and their behaviors as selective turn-on fluorescence probes toward singlet oxygen ($^1O_2$) and hypochlorite (Figure 1). In Scheme 1, we represented the detection strategies of ROS with turn-on fluorescence of self-assembled probe **1**. The self-assembled probe **1** with turn-off changed to turn-on through morphological transformation from sphere to continuously networked fibrous structures.
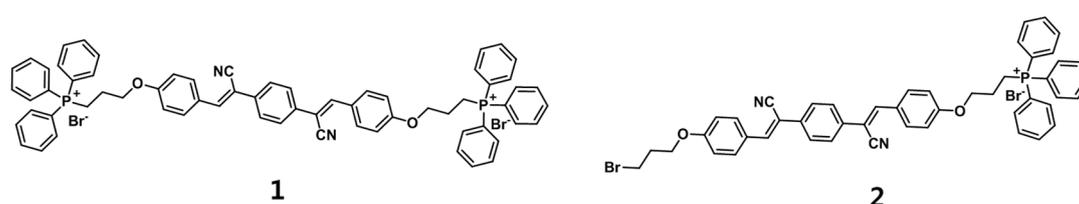
Figure 1. Chemical structures of probes **1** and **2**.
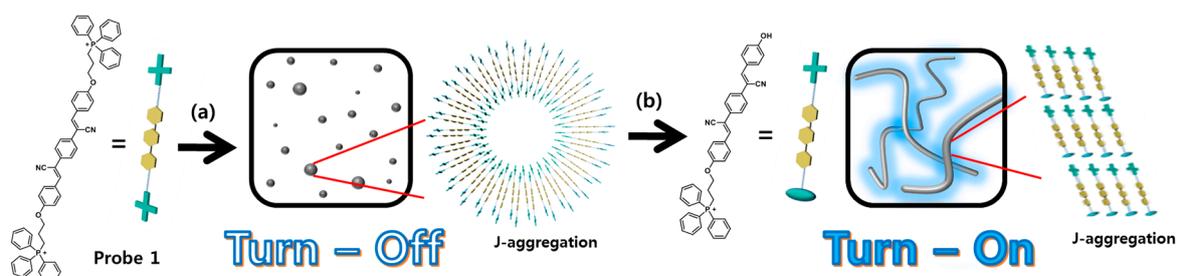
Scheme 1. Morphological change-based turn-on system for ROS detection: (**a**) formation of self-assembled spherical structure (gray sphere) and (**b**) morphological change into the fiber structure (gray ribbon) by ROS recognition.

2. Materials and Methods

2.1. Reagents and Instruments

All reagents were purchased from Sigma-Aldrich (Yongin, South Korea). The solvent was purchased from Samchun Pure Chemicals (Pyeongtaek, South Korea) and used with further purification. ^{1}H and ^{13}C NMR spectra were measured using a Bruker DRX 300 spectrometer (Bruker). Furthermore, the mass spectra were measured using a JEOL JMS-700 mass spectrometer (JEOL Ltd., Tokyo, Japan). In addition, a Thermo Evolution 600 UV-vis spectrophotometer (Thermo Fisher Scientific, Waltham, MA, USA) was used to obtain the absorption spectra in the solution, and the fluorescence spectra were recorded using a RF-5301PC spectrophotometer (Shimadzu Corp., Kyoto, Japan).

2.2. Synthesis of Compound 3

Compound **3** was synthesized using a previously reported method. Here 1,3-dibromopropane (2.5 mL, 24.57 mmol), *p*-hydroxybenzaldehyde (2.0 g, 16.38 mmol), and K_2CO_3 (3.39 g, 24.57 mmol) were dissolved in acetone (75 mL). The reaction mixture was heated to 50 °C for 12 h. Then, the reaction mixture was cooled to room temperature, filtered, and concentrated under reduced pressure. The crude product was purified using silica gel and eluted with ethyl acetate and hexane of compound **3**: ^{1}H NMR (300 MHz, DMSO-d_6) δ 9.88 (s, 1H), 7.90–7.86 (d, 2H), 7.17–7.14 (d, 2H), 4.23–4.19 (t, 2H), 3.70–3.66 (t, 2H), 2.32–2.24 (m, 2H); ^{13}C NMR (75 MHz, DMSO-d_6) δ 190.89, 163.89, 132.18, 130.38, 118.48, 114.99, 69.20, 65.91, 32.27, 29.78.

2.3. Synthesis of Compound 2

Compound **3** (1.71 g, 7.03 mmol) and p-xylene dicyanide (0.5 g, 3.2 mmol) were dissolved in ethanol (30 mL). Sodium methoxide (0.35 g, 6.4 mmol) was added, and the solution was heated at reflux under N_2 atmosphere. After 12, the reaction mixture was then cooled to room temperature, and the solid was filtered and washed with methanol: (yellow solid, 55% yield); ^{1}H NMR (300 MHz, DMSO-d_6), δ (ppm): 8.07 (s, 2H), 8.00–7.97 (d, 4H), 7.86 (s, 4 H), 7.17–7.14 (d, 4H), 4.22–4.18 (t, 4H), 3.70–3.68 (t, 4H), 2.34–2.25 (m, 4H); ^{13}C NMR (75 MHz, DMSO-d_6), δ (ppm): 160.3, 143.2, 134.4, 131.7, 126.0, 124.8, 118.5, 116.0, 105.1.

2.4. Synthesis of Probe 1

Compound **2** (0.5 g, 0.82 mmol) was dissolved in acetonitrile (100 mL) with triphenylphosphine (1.3 g, 4.92 mmol). The mixture was heated to 85 °C for 48 h. Acetonitrile was removed under vacuum, and the precipitated yellow solid was collected by recrystallization. Then, the product was purified by flash chromatography using dichloromethane: (yellow solid, 61% yield); ^{1}H NMR (300 MHz, DMSO-d_6), δ (ppm): 8.10 (s, 2H), 8.00–7.76 (m, 42H), 7.14–7.12 (t, 4H), 4.25–4.18 (t, 4H), 3.81–3.71 (t, 4H), 2.02(s, 4H); ^{13}C NMR (75 MHz, DMSO-d_6), δ (ppm): 160.6, 143.4, 165.5, 134.8, 134.2, 134.1, 131.8, 130.9, 130.7, 127.0, 126.6, 119.4, 118.7, 118.2, 115.6, 106.9; FT-IR (cm^{-1}): 2209, 1599, 1510, 1434, 1245, 1183, 1110; ESI-MS (m/z): 485.42 [**1** + H]$^{2+}$, 1052.00 [**1** + Br]$^+$.

2.5. Synthesis of Probe 2

Compound **2** (0.5 g, 0.82 mmol) was dissolved in acetonitrile (100 mL) with triphenylphosphine (0.43 g, 1.64 mmol). The mixture was heated to 85 °C for 48 h. Acetonitrile was removed under vacuum, and the precipitated yellow solid was collected by recrystallization. Then, the product was purified by flash chromatography using dichloromethane/methanol (10:1). (yellow solid, 22.3% yield); ^{1}H NMR (300 MHz, DMSO-d_6), δ (ppm): 8.09 (s, 2H), 8.01–7.76 (m, 23H), 7.14–7.11 (s, 4H), 4.25–4.19 (s, 4H), 3.84–3.67 (s, 4H), 2.23–2.21 (s, 2H), 2.05 (s, 2H); ^{13}C NMR (75 MHz, DMSO-d_6), δ (ppm): 161.5, 143.9,

136.1, 135.9, 130.8, 130.1, 126.2, 119.2, 117.6, 107.7, 68.2, 33.8, 31.2; FT-IR (cm^{-1}): 2214, 1594, 1508, 1434, 1508, 1434, 1259, 1176, 1109, 687; ESI-MS (m/z): 789.17 [**2** + H]$^{+}$.

2.6. Synthesis of *1-Ref*

1-Ref was synthesized by the reported method [S1].; ^{1}H NMR (300 MHz, DMSO-d_6), δ (ppm): 10.33 (s, 2H), 7.98 (s, 2H), 7.92–7.87 (d, 4H), 7.82 (s, 4H), 6.95 (s, 2H), 2); ^{13}C NMR (75 MHz, DMSO-d_6), δ (ppm): 160.4, 143.0, 133.4, 132.7, 126.5, 125.9, 117.4, 117.0, 105.2; FT-IR (cm^{-1}): 3200, 2222, 1609, 1592, 1514, 1440, 1300, 1173.

2.7. Fluorescence Spectroscopy

A 1-cm long cuvette was used in the fluorescence assay. The sample was excited at 367 nm, and the emission was collected from 500 nm. ROS detection experiments were performed three times. To detect the ROS by probe **1**, 1 mL of standard solution (pH = 7.4) was first added to the cuvette. Then, the hydroxyl radical was generated via Fenton reaction with different amounts of Fe^{2+} and H$_2$O$_2$ (Fe^{2+}/H$_2$O$_2$ = 1:10). After incubation with the probe for 15 min. For the selectivity experiment, hydroxyl radical ($^{\bullet}$OH) was generated via Fenton reaction (Fe^{2+}/H$_2$O$_2$ = 200 μM, 2000 μM). Superoxide anion (O$_2^{\bullet-}$) was derived from dissolved KO$_2$ (200 μM) in the DMSO solution. Hypochlorite anion (ClO$^-$) was provided by NaClO (200 μM). Nitric oxide (NO) and nitroxyl (HNO) were derived from a solution of S-nitroso-N-acetyl-DL-penicillamine and Angeli's salt, respectively. ^{1}O$_2$ was generated by the reaction of H$_2$O$_2$ (200 μM) with NaClO (200 μM). Other species (10 equiv.) were prepared by dissolving in aqueous solutions at pH 7.4. All experiments were performed after incubation with the appropriate ROS/RNS for 10 min at room temperature.

2.8. Determination of Limit of Detection

The limit of detection (LOD) of probe **1** for ClO$^-$ and ^{1}O$_2$ was determined as 33 μM and 56 μM, respectively. The LOD was calculated using the following equation, where σ is the standard deviation of the blank measurements and s is the slope of the calibration plot.

$$\text{LOD} = 3 \times \sigma/\text{s} \tag{1}$$

3. Results and Discussion

3.1. Characterization of Self-Assembled Probes *1* and *2*

Probes **1** and **2** were synthesized by a reaction of bromine-modified dicyanostilbene with TPP in acetonitrile following a previously reported method. Compounds **1** and **2** were confirmed by ^{1}H and ^{13}C NMR, ESI-MS, and FT-IR spectroscopy (Figure S1). ^{1}H NMR data indicate that probes **1** and **2** demonstrated only a (Z)-form originating from the alkene peak at 8.04 in the dicyanostilbene moiety.

Since TPP-appended dicyanostilbene derivatives often demonstrate amphiphilic properties [26]. we observed the self-assembling behaviors in aqueous solution. In the aqueous solution (1% DMSO) at 25 °C, the UV-Vis absorption bands of **1** (25 μM) and **2** (6.25 μM) appeared at 360 nm and 371 nm, respectively. The UV-Vis absorption bands originated from π-π transitions of the dicyanostilbene moiety and shifted to a longer wavelength by increasing the temperatures of the aqueous solution (1% DMSO) (Figure 2). These red shifts were due to the formation of self-assembly via *J*-aggregation [27]. Note that the λ$_{max}$ shift of probe **2** was smaller than that of probe **1**, which indicates that, compared to probe **2**, probe **1** formed more stable self-assembly in aqueous solution. The fluorescence spectra of probes **1** and **2** (excitation wavelength: **1** at 360 nm and **2** at 371 nm) were obtained by change of temperature (Figure S2). Weak fluorescence bands for probes **1** and **2** were observed at 512 nm due to the PET from fluorophore to TPP [28]. Due to the change from self-assembly to de-assembly, the fluorescence intensities decreased as the temperature increased. The fluorescence intensity of probe **1** decreased at 35–45 °C, whereas the fluorescence intensity of probe **2** decreased

at 25–35 °C. We also measured the temperature-dependent ^{1}H NMR spectra of probes **1** and **2** to obtain the key factor in the formation of self-assembly in DMSO-d_6/D$_2$O (99/1, *v/v*%) (Figure S3). The tendency of the chemical shift of an alkene peak in probe **1** was similar to that of probe **2**; however, the shift of probe **1** was greater than that of probe **2**. In addition, the interaction between alkene groups may affect enhancement of self-assembly stability. However, compared to probe **2**, the stabilization enhancement of self-assembled probe **1** led to intrinsic fluorescence quenching due to the reduced distance between dicyanostilbene and TPP via *J*-aggregation, as well as the effect of TPP groups inducing PET from dicyanostilbene.
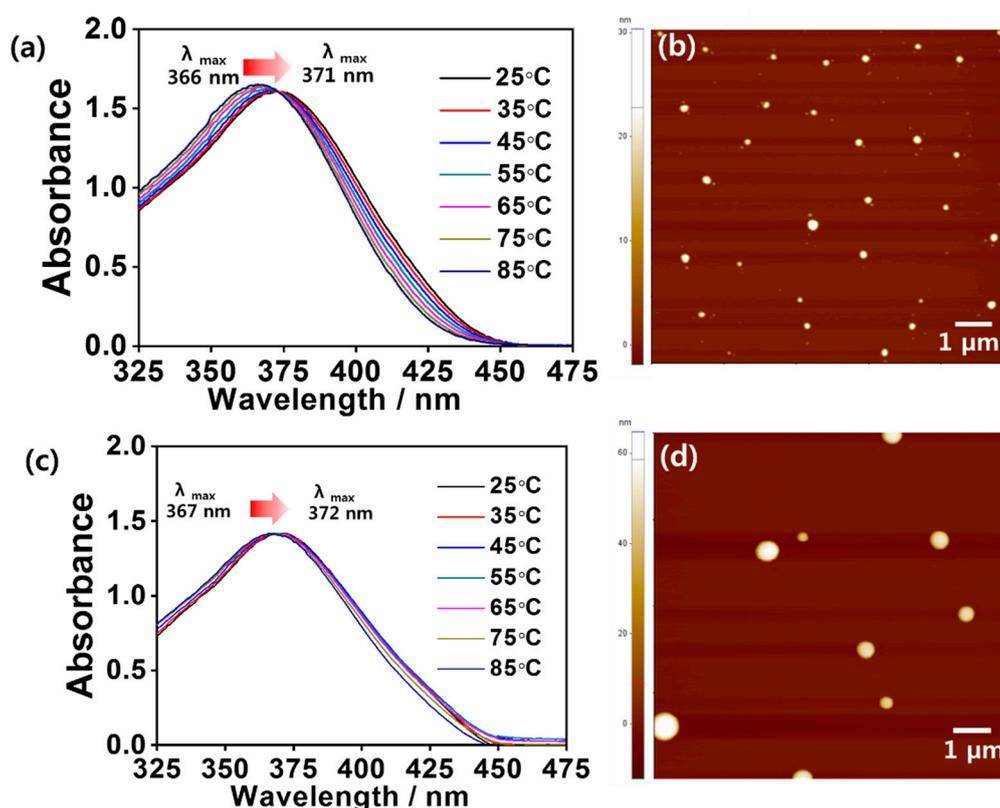
Figure 2. Temperature dependent UV–VIS spectra of probes (**a**) **1** (25 µM) and (**c**) **2** (6.25 µM) in DMSO/H$_2$O (1/99, *v/v*%). AFM images of probes (**b**) **1** (100 µM) and (**d**) **2** (100 µM).

We also observed morphologies of self-assembled **1** and **2** using atomic force microscopy (AFM) (Figures 2 and S9). The AFM image of probe **1** showed a spherical structure with a diameter of ca. 22–32 nm (Figures 2b and S9a). The spherical nanoparticle should form by intermolecular dipole-dipole interaction and π-π stacking [29]. Similarly, probe **2** showed a spherical structure with a diameter of ca. 53–63 nm (Figures 2d and S9b). The size difference of self-assembled spheres **1** and **2** was due to the TPP group and the binding strength of the π-π interaction between the alkene groups, as shown by the ^{1}H NMR data. Thus, we recognize that the size of the self-assembled spherical nanoparticles was determined by the strength of the intermolecular interactions. Based on UV-Vis, PL, and ^{1}H NMR experiments, we conclude that **1** and **2** formed self-assembled spherical nanoparticles by *J*-aggregation with dipole-dipole interaction between the alkene groups in the dicyanostilbene moiety. The stability of self-assembled **1** was greater than that of self-assembled probe **2** (i.e., the TPP substitution effect accompanied fluorescence turn-off). We inserted a table involving summarized characteristics of the probes **1** and **2** (Table S1).

3.2. ROS-Sensing Ability of Self-Assembled Probes 1 and 2 in Aqueous Solution

Self-assembled probes **1** and **2** with negligible fluorescence emission bands were used in aqueous solution to apply a turn-on fluorescence probe to highly ROS. The fluorescence spectral changes of self-assembled probe **1** were observed upon addition of several species related to ROS, such as singlet oxygen (10 equiv. of $^1O_2$) and other ROS (10 equiv. of O_2^-, H_2O_2, NO, TBHP, ClO^-, $^\bullet OH$, GSH, cysteine, histidine, K^+, and Na^+) in water at pH 7.4 (Figure 3). Upon treatment with 10 equiv. of $^1O_2$ and ClO^-, a marked strong green emission at 520 nm was observed in under 5 min, indicating that $^1O_2$ and ClO^- reacted with self-assembled **1** rapidly at room temperature. In addition, the fluorescence intensity of self-assembled **1** in the presence of $^1O_2$ and ClO^- was enhanced by 2.3 and 2.7 times, respectively, compared to self-assembled **1** in the absence of $^1O_2$ and ClO^-. In contrast, significant selective changes in the emission were not observed upon addition of O_2^-, H_2O_2, NO, TBHP, ClO^-, $^\bullet OH$, GSH, cysteine, histidine, K^+, and Na^+ (Figure 3), indicating that these ROS species, amino acids, and metal ions did not react to **1**. The large difference in the fluorescence images between $^1O_2$, ClO^-, and other ROS was observed after treatment of **1** (Figure 3). Their fluorescence enhancement of self-assembled **1** in the presence of $^1O_2$ or ClO^- indicated that the complex between **1** and $^1O_2$ or ClO^- hinders PET [18]. The non-emission of self-assembled **1** upon addition of other oxide species, such as O_2^- and NO, may be less reactive with 1 than that when $^1O_2$ or ClO^- are added [30]. The sensing ability of self-assembled **2** was also evaluated under the same conditions. Self-assembled **2** exhibited fluorescence enhancement upon addition of O_2^-, $^\bullet OH$, and ClO^-. A hydrolysis reaction of the bromide group in self-assembled **2** with O_2^- or $^\bullet OH$ did occur. The hydroxyl group in self-assembled **2** might induce fluorescence turn-off through the electron transfer mechanism [31]. Therefore, the fluorescence enhancement effect of self-assembled **2** was weaker than that of **1**. The slight turn-on effects of **2** in the presence of O_2^-, $^\bullet OH$, and ClO^- may be caused by the reaction of a –Br group with ROS (O_2^-, $^\bullet OH$, and ClO^-), as indicated by the IR data (Figure S4).
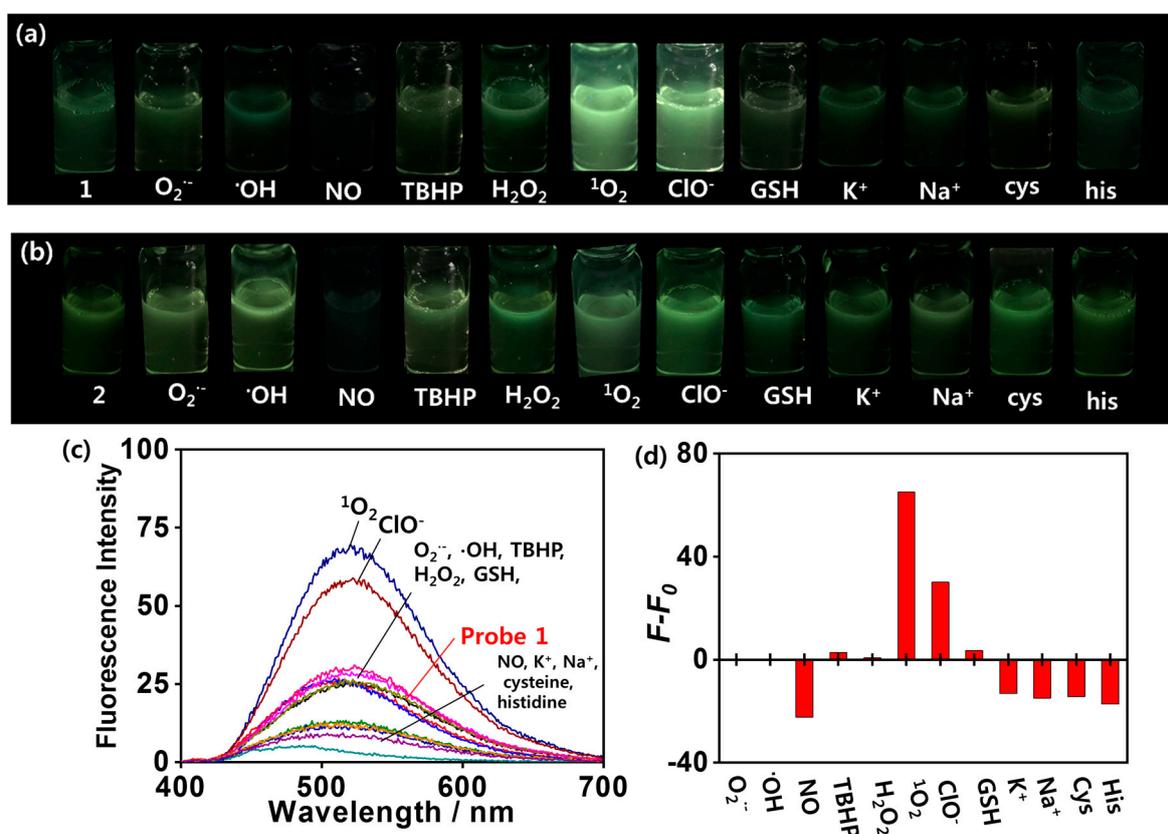
Figure 3. *Cont.*
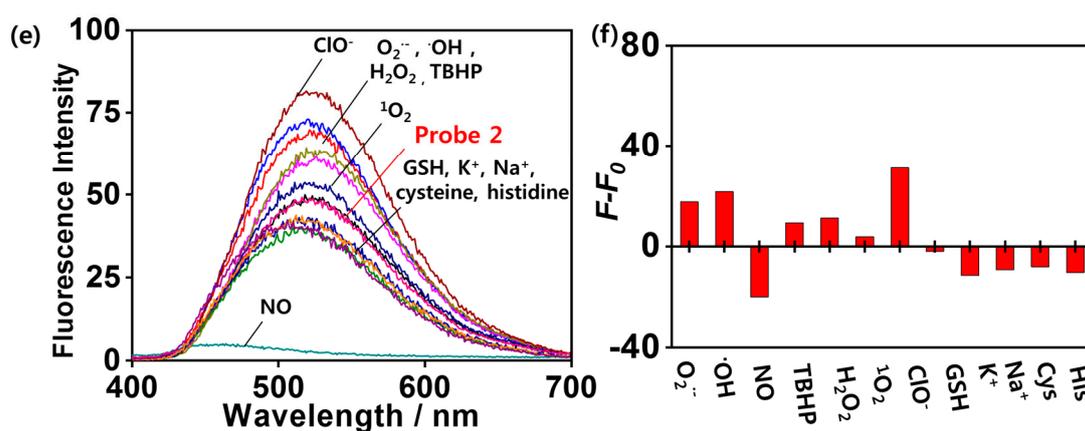
Figure 3. Photographs of (**a**) **1** (25 μM) and (**b**) **2** (6.25 μM) with ROS (10 equiv.), metal ions (10 equiv.), or amino acids (10 equiv.) in DMSO/H$_2$O (1/99, *v*/*v*%) under UV lamp. Fluorescence spectra (Excitation wavelength: 360 nm for probe **1** and 371 nm for probe **2**) of (**c**) **1** and (**e**) **2** with ROS (10 equiv.), metal ions (10 equiv.), or amino acids (10 equiv.) in DMSO/H$_2$O (1/99, *v*/*v*%). Fluorescence intensity of probes (**d**) **1** and (**f**) **2** in the presence of ROS, metal ions, and amino acids in DMSO/H$_2$O (1/99, *v*/*v*%).

To quantitatively investigate the reactivity and spectral changes of **1** (25 μM) upon addition of $^1O_2$ and ClO$^-$, fluorescence titrations were performed by adding $^1O_2$ and ClO$^-$ (0–375 μM) in water (containing 1% DMSO) at room temperature (Figure 4). The fluorescence intensity of **1** at 520 nm, which originates from dicyanostilbene moiety, was enhanced drastically during the titration process. In addition, at less than **2** equiv. of $^1O_2$ and ClO$^-$, an excellent nonlinear correction between fluorescence intensity and the concentration of $^1O_2$ and ClO$^-$ was obtained with R^2 = 0.9923 for $^1O_2$ and R^2 = 0.9633 for ClO$^-$, indicating that the ratio of fluorescence intensity at 520 nm was enhanced as a nonlinear function of $^1O_2$ and ClO$^-$ concentration. This turn-on mechanism can be attributed to the cooperative effects of AIEE of dicyanostilbene and blocking of the photoinduced electron transfer process. The detection limits of self-assembled **1** for ClO$^-$ and $^1O_2$ were 33 μM and 56 μM, respectively (Figure S5) [S2].

To further evaluate the utility of **1** as a selective fluorescence probe for $^1O_2$ and ClO$^-$, the competition-based fluorescence emission changes of self-assembled **1** upon addition of various biologically relevant species and ROS (i.e., ClO$^-$, $^1O_2$, O$_2^-$, H$_2$O$_2$, NO, TBHP, ClO$^-$, $^\bullet$OH, GSH, cysteine, histidine, K$^+$, and Na$^+$) were investigated in aqueous solution (Figure S6). In binary system, probe **1** showed a strong green emission with $^1O_2$ or ClO$^-$ except for cysteine, histidine and NO. The emission change with cysteine was due to that the phenoxy oxygen of **1** may be interacted with -SH group in cysteine [32,33]. In addition, histidine molecules were due to their bioactive properties inducing the reaction of histidine with $^1O_2$ or ClO$^-$ prior to probe **1** [33]. Low turn-on emission of probe **1** in presence of K$^+$ and Na$^+$ ions can be caused by the charge interaction of cation with $^1O_2$ or ClO$^-$ prior to react with probe **1**. As expected, the fluorescence intensities of self-assembled **1** in the presence of $^1O_2$ and ClO$^-$ were unchanged by treatment of other species, such as O$_2^-$, H$_2$O$_2$, NO, TBHP, $^\bullet$OH, GSH, K$^+$, and Na$^+$, indicating that self-assembled **1** is a new selective turn-on fluorescence probe of $^1O_2$ and ClO$^-$ in a mixture of other species.
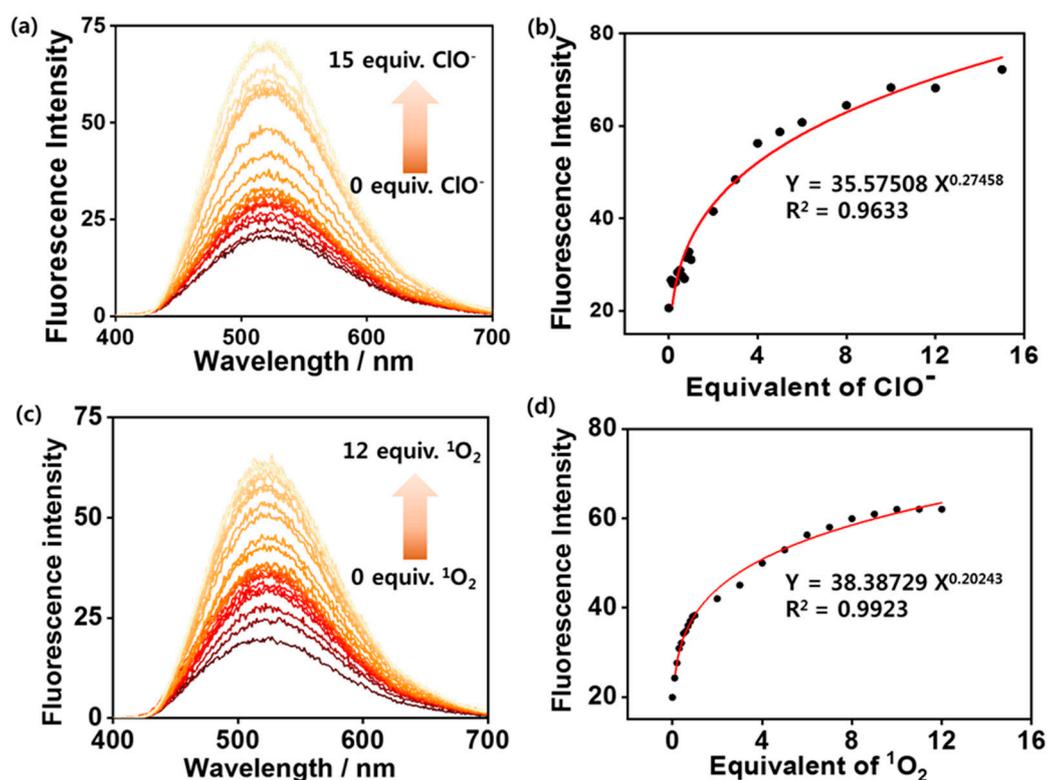
Figure 4. Fluorescence spectra (Excitation wavelength: 360 nm for probe **1**) of **1** (25 μM) in the presence of various concentrations of (**a**) ClO^- (0–375 μM) and (**c**) $^1O_2$ (0–300 μM) in DMSO/H_2O (1/99, *v/v*%). Plot for fluorescence intensity of **1** upon addition of (**b**) ClO^- and (**d**) $^1O_2$.

3.3. ROS-Mediated Fluorescence Turn-On Mechanism of Self-Assembled Probe **1** in Aqueous Solution

The mechanism of the reaction between self-assembled **1** and $^1O_2$ or ClO^- was further studied. First, the bonding cleavage of **1** upon addition of $^1O_2$ or ClO^- was confirmed at the molecular level. The mechanism of the reaction between self-assembled **1** and $^1O_2$ or ClO^- was further studied. First, the bonding cleavage of **1** upon addition of $^1O_2$ or ClO^- was confirmed at the molecular level. The shape of the UV-Vis spectra of self-assembled probe **1** treated with $^1O_2$ or ClO^- was almost same to that without $^1O_2$ or ClO^- (Figure S7). On the other hand, the molecular structure of dicyanostilbene was conserved when $^1O_2$ or ClO^- was added to self-assembled **1**. We observed FAB-Mass and IR spectral changes of **1** with $^1O_2$ or ClO^- (Figure S7). After treatment with $^1O_2$ or ClO^-, a mass value of 667.3 was obtained. This value indicates that the oxygen atom adjacent at dicyanostilbene reacted with $^1O_2$ or ClO^- and then formed a phenol moiety (Figure S7). Furthermore, the IR spectra of **1** upon addition of $^1O_2$ or ClO^- showed new peaks at 900–1100 cm^{-1} (OH bending vibration), and peaks in the range of 3100–3700 cm^{-1} were widened due to the formation of the phenolic OH group in **1** (Figure S7). In addition, by comparing the IR data (1000–2400 cm^{-1}) of self-assembled **1** with or without analyte, we confirmed that the structure of the dicyanostilbene moiety was conserved while self-assembled **1** reacted to $^1O_2$ or ClO^-. A dicyanostilbene derivative possessing OH group (**1-Ref**) was synthesized to assign OH groups on IR and NMR data (Figures S7A and S8). In Figures S7 and S8, the OH groups the product obtained from probe **1** in the presence of $^1O_2$ or ClO^- correspond with the OH peaks compound **1-Ref**. However, the product obtained from probe **1** with $^1O_2$ or ClO^- was produced one −OH as shown in Figure S8, but not two −OH groups. We measured zeta potential of probe **1** and probe **1** treated with $^1O_2$ or ClO^- to further confirm about its structure change (Figure S10). The zeta potential of the probe **1** was determined to be 32.46 mV; however, the zeta potential of the probe **1** treated with $^1O_2$ or ClO^- was 21.43 mV and 23.16 mV respectively; this was due to the formation of

OH group. These results strongly indicated that the OH group originated from the reaction of probe **1** with $^1O_2$ or ClO^- had been successfully formed.

Furthermore, the morphological change of self-assembled **1** was observed by treatment with $^1O_2$ or ClO^- by AFM. After treatment with $^1O_2$ or ClO^-, the spherical nanoparticle formed via self-assembly of **1** changed to a fiber structure (Figures 5 and S9c).
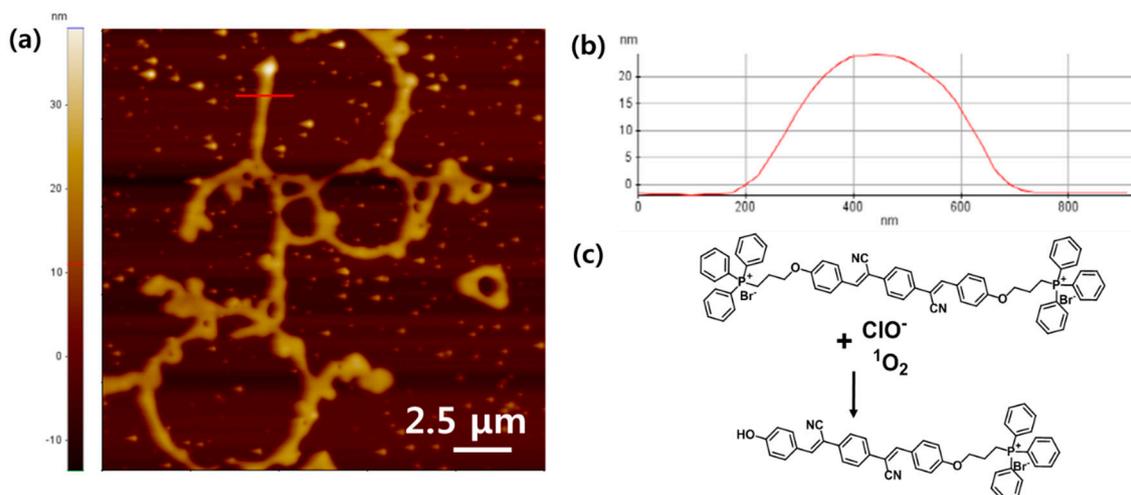
Figure 5. (**a**) AFM image of **1** (100 μM) in DMSO/H$_2$O (1/99, *v*/*v*%) after adding ClO^- or $^1O_2$. (**b**) Height and width of nanofiber (**a**). (**c**) Mechanism of **1** after adding ClO^- or $^1O_2$. (ClO^--treated probe **1** and $^1O_2$-treated probe **1** were shown similar morphologies).

Therefore, we propose a schematic illustration of the reaction-based morphological change of self-assembled **1** during the reaction that progressed upon adding $^1O_2$ or ClO^- (Figure 5). To the best of our knowledge, the selectivity of probe **1** for $^1O_2$ could be described by two-step reactions. First, an aliphatic carbon adjacent to the oxygen atom was attacked by $^1O_2$ [34]. Then, water reacted with the $^1O_2$-derived activated group to form a hydroxyl end group in the dicyanostilbene moiety. Due to the structural stabilization effect of the fully-conjugated dicyanostilbene moiety, alkene groups in dicyanostilbene may be less reactive than the carbon atoms adjacent to the oxygen atom of probe **1**.

4. Conclusions

We have synthesized novel triphenylphosphonium-strapped dicyanostilbene derivatives (probes **1** and **2**) and characterized their self-assembly properties by using spectroscopic analysis. Owing to the TPP substitution effects, probe **1** were formed more stable self-assembly than that of probe **2**. The spherical structure of self-assembled probe **1** were shown selectively turn-on fluorescence upon addition of $^1O_2$ or ClO^-. Moreover, the morphology of self-assembled probe **1** was changed from sphere to fibrous structures in the presence of $^1O_2$ or ClO^-. We also proved that the generation of OH group-substituted TPP-dicyanostilbene caused by the reaction between oxygen atoms adjacent dicyanostilbene of probe **1** and $^1O_2$ or ClO^-. Thus, we could propose continuous fibrous-mediated AIEE effect-based turn-on sensing mechanism of probe **1** for $^1O_2$ or ClO^- by using molecular and nanometer level analysis. Based on our results, it is expected that a nanostructure change-derived turn-on sensing strategy for $^1O_2$ or ClO^- may offer a new approach to develop methods in biological and environmental subjects.

Author Contributions: Conceptualization, W.C. and N.Y.L.; Data curation, W.C.; Formal analysis, W.C. and N.Y.L.; Investigation, W.C., N.Y.L. and H.C.; Methodology, H.C.; Project administration, H.C. and M.L.S.; Supervision, M.L.S., J.A. and J.H.J.; Writing-original draft, J.A.; Writing-review & editing, J.A. and J.H.J.

Conflicts of Interest: The authors declare no conflict of interest.

References

1. Zhao, X.; Zheng, H.; Qu, D.; Jiang, H.; Fan, W.; Sun, Y.; Xu, Y. A supramolecular approach towards strong and tough polymer nanocomposite fibers. *RSC Adv.* **2018**, *8*, 10361–10366. [CrossRef]

2. Cherumukkil, S.; Vedhanarayanan, B.; Das, G.; Praveen, V.K.; Ajayaghosh, A. Self-assembly of Bodipy-derived extended π-Systems. *Bull. Chem. Soc. Jpn.* **2018**, *91*, 100–120. [CrossRef]

3. Shimizu, T. Self-assembly of discrete organic nanotubes. *Bull. Chem. Soc. Jpn.* **2018**, *91*, 623–668. [CrossRef]

4. Ariga, K.; Nishikawa, M.; Mori, T.; Takeya, J.; Shrestha, L.K.; Hill, J.P. Self-assembly as a key player for materials nanoarchitectonics. *Sci. Technol. Adv. Mater.* **2018**. [CrossRef]

5. Li, S.; Tian, T.; Zhang, T.; Cai, X.; Lin, Y. Advances in biological applications of self-assembled DNA tetrahedral nanostructures. *Mater. Today* **2018**. [CrossRef]

6. Hu, Z.-T.; Chen, Z.; Goei, R.; Wu, W.; Lim, T.-T. Magnetically recyclable Bi/Fe-based hierarchical nanostructures via self-assembly for environmental decontamination. *Nanoscale* **2016**, *8*, 12736–12746. [CrossRef] [PubMed]

7. Wang, H.; Hu, L.; Du, W.; Tian, X.; Hu, Z.; Zhang, Q.; Zhou, H.; Wu, J.; Uvdal, K.; Tian, Y. Mitochondria-targeted iridium (III) complexes as two-photon fluorogenic probes of cysteine/homocysteine. *Sens. Actuators B* **2018**, *255*, 408–415. [CrossRef]

8. Wong, J.K.H.; Todd, M.H.; Rutledge, P.J. Recent advances in macrocyclic fluorescent probes for ion sensing. *Molecules* **2017**, *22*, 200. [CrossRef] [PubMed]

9. Mandal, K.; Jana, D.; Ghorai, B.K.; Jana, N.R. Functionalized chitosan with self-assembly induced and subcellular localization-dependent fluorescence 'switch on' property. *New J. Chem.* **2018**, *42*, 5774–5784. [CrossRef]

10. Shi, J.; Wu, Y.; Tong, B.; Zhi, J.; Dong, Y. Tunable fluorescence upon aggregation: Photophysical properties of cationic conjugated polyelectrolytes containing AIE and ACQ units and their use in the dual-channel quantification of heparin. *Sens. Actuators B* **2014**, *197*, 334–341. [CrossRef]

11. Chen, X.; Tian, X.; Shin, I.; Yoon, J. Fluorescent and luminescent probes for detection of reactive oxygen and nitrogen species. *Chem. Soc. Rev.* **2011**, *40*, 4783–4804. [PubMed]

12. Jin, L.; Xu, M.; Jiang, H.; Wang, W.; Wang, Q. A simple fluorescein derived colorimetric and fluorescent 'off-on' sensor for the detection of hypochlorite. *Anal. Methods* **2018**, *10*, 4562–4569. [CrossRef]

13. Li, K.; Hou, J.-T.; Yang, J.; Yu, X.-Q. A tumor-specific and mitochondria-targeted fluorescent probe for real-time sensing of hypochlorite in living cells. *Chem. Commun.* **2017**, *53*, 5539–5541. [CrossRef] [PubMed]

14. Pavelescu, L.A.; Iordache, M.-M.; Savopol, T.; Kovacs, E.; Moisescu, M.G. A new technique for evaluating reactive oxygen species generation. *Biointerface Res. Appl. Chem.* **2015**, *5*, 1003–1006.

15. Jiao, X.; Li, Y.; Niu, J.; Xie, X.; Wang, X.; Tang, B. Small-Molecule Fluorescent Probes for Imaging and Detection of Reactive Oxygen, Nitrogen, and Sulfur Species in Biological Systems. *Anal. Chem.* **2018**, *90*, 533–555. [CrossRef]

16. Chang, C.; Wang, F.; Qiang, J.; Zhang, Z.; Chen, Y.; Zhang, W.; Wang, Y.; Chen, X. Benzothiazole-based fluorescent sensor for hypochlorite detection and its application for biological imaging. *Sens. Actuators B* **2017**, *243*, 22–28. [CrossRef]

17. Yu, H.; Liu, X.; Wu, Q.; Li, Q.; Wang, S.; Guo, Y. A new rhodamine-based fluorescent probe for the detection of singlet oxygen. *Chem. Lett.* **2015**, *44*, 244–246. [CrossRef]

18. Liu, H.-W.; Xu, S.; Wang, P.; Hu, X.-X.; Zhang, J.; Yuan, L.; Zhang, X.-B.; Tan, W. An efficient two-photon fluorescent probe for monitoring mitochondrial singlet oxygen in tissues during photodynamic therapy. *Chem. Commun.* **2016**, *52*, 12330–12333. [CrossRef]

19. You, Y.; Cho, E.J.; Kwon, H.; Hwang, J.; Lee, S.E. A singlet oxygen photosensitizer enables photoluminescent monitoring of singlet oxygen doses. *Chem. Commun.* **2016**, *52*, 780–783. [CrossRef]

20. Mulay, S.V.; Choi, M.; Jang, Y.J.; Kim, Y.; Jon, S.; Churchill, D.G. Enhanced Fluorescence Turn-on Imaging of Hypochlorous Acid in Living Immune and Cancer Cells. *Chem. Eur. J.* **2016**, *22*, 9642–9648. [CrossRef]

21. Wang, L.; Yang, L.; Zhu, L.; Cao, D.; Li, L. Synthesis, characterization and fluorescence "turn-on" detection of BSA based on the cationic poly(diketopyrrolopyrrole-co-ethynylfluorene) through deaggregating process. *Sens. Actuators B* **2016**, *231*, 733–743. [CrossRef]

22. Alifu, N.; Dong, X.; Li, D.; Sun, X.; Zebibula, A.; Zhang, D.; Zhang, G.; Qian, J. Aggregation-induced emission nanoparticles as photosensitizer for two-photon photodynamic therapy. *Mater. Chem. Front.* **2017**, *1*, 1746–1753. [CrossRef]

23. En, Y.; Zhang, R.; Yan, C.; Wang, T.; Cheng, H.; Cheng, X. Self-assembly, AIEE and mechanochromic properties of amphiphilic α-cyanostilbene derivatives. *Tetrahedron* **2017**, *73*, 5253–5259.

24. Luo, C.; Liu, Y.; Zhang, Q.; Cai, X. Hyperbranched conjugated polymers containing 1,3-butadiene units: Metal-free catalyzed synthesis and selective chemosensors for Fe^{3+} ions. *RSC Adv.* **2017**, *7*, 12269–12276. [CrossRef]

25. Xiao, H.; Li, J.; Zhao, J.; Yin, G.; Quan, Y.; Wang, J.; Wang, R. A colorimetric and ratiometric fluorescent probe for ClO- targeting in mitochondria and its application in vivo. *J. Mater. Chem. B* **2015**, *3*, 1633–1638. [CrossRef]

26. Kim, K.Y.; Jin, H.; Park, J.; Jung, S.H.; Lee, J.H.; Park, H.; Kim, S.K.; Bae, J.; Jung, J.H. Mitochondria-targeting self-assembled nanoparticles derived from triphenylphosphonium-conjugated cyanostilbene enable site-specific imaging and anticancer drug delivery. *Nano Res.* **2018**, *11*, 1082–1098. [CrossRef]

27. Tay-Agbozo, S.; Street, S.; Kispert, L.D. The carotenoid bixin: Optical studies of aggregation in polar/water solvents. *J. Photochem. Photobiol. A* **2018**, *362*, 31–39. [CrossRef]

28. Yuan, H.; Cho, H.; Chen, H.H.; Panagia, M.; Sosnovik, D.E.; Josephson, L. Fluorescent and radiolabeled triphenylphosphonium probes for imaging mitochondria. *Chem. Commun.* **2013**, *49*, 10361–10363. [CrossRef]

29. Van Herrikhuyzen, J.; Willems, R.; George, S.J.; Flipse, C.; Gielen, J.C.; Christianen, P.C.M.; Schenning, A.P.H.J.; Meskers, S.C.J. Atomic Force Microscopy Nanomanipulation of Shape Persistent, Spherical, Self-Assembled Aggregates of Gold Nanoparticles. *ACS Nano* **2010**, *4*, 6501–6508. [CrossRef]

30. Hu, J.J.; Wong, N.-K.; Lu, M.-Y.; Chen, X.; Ye, S.; Zhao, A.Q.; Gao, P.; Kao, R.Y.-T.; Shen, J.; Yang, D. HKOCl-3: A fluorescent hypochlorous acid probe for live-cell and in vivo imaging and quantitative application in flow cytometry and a 96-well microplate assay. *Chem. Sci.* **2016**, *7*, 2094–2099. [CrossRef]

31. Zhang, H.; Liu, J.; Liu, C.; Yu, P.; Sun, M.; Yan, X.; Guo, J.-P.; Guo, W. Imaging lysosomal highly reactive oxygen species and lighting up cancer cells and tumors enabled by a Si-rhodamine-based near-infrared fluorescent probe. *Biomaterials* **2017**, *133*, 60–69. [CrossRef] [PubMed]

32. Njeri, C.W.; Ellis, H.R. Shifting redox states of the iron center partitions CDO between crosslink formation or cysteine oxidation. *Arch. Biochem. Biophys.* **2014**, *558*, 61–69. [CrossRef] [PubMed]

33. Hou, J.; Zhang, F.; Yan, X.; Wang, L.; Yan, J.; Ding, H.; Ding, L. Sensitive detection of biothiols and histidine based on the recovered fluorescence of the carbon quantum dots-Hg (II) system. *Anal. Chim. Acta* **2015**, *859*, 72–78. [CrossRef] [PubMed]

34. Sagadevan, A.; Hwang, K.C.; Su, M.-D. Singlet oxygen-mediated selective C–H bond hydroperoxidation of ethereal hydrocarbons. *Nat. Commun.* **2017**, *8*, 1812. [CrossRef] [PubMed]